FOCUSED TOPIC

Virulent Disease Epidemics Can Increase Host Density by Depressing Foraging of Hosts*

Rachel M. Penczykowski,[1,2,†] Marta S. Shocket,[3,‡] Jessica Housley Ochs,[1] Brian C. P. Lemanski,[1,4] Hema Sundar,[1] Meghan A. Duffy,[1,5] and Spencer R. Hall[3]

1. School of Biology, Georgia Institute of Technology, Atlanta, Georgia 30332;   2. Department of Biology, Washington University in St. Louis, St. Louis, Missouri 63130;   3. Department of Biology, Indiana University, Bloomington, Indiana 47405;   4. Department of Biology, Colgate University, Hamilton, New York 13346;   5. Department of Ecology and Evolutionary Biology, University of Michigan, Ann Arbor, Michigan 48109

ABSTRACT: All else equal, parasites that harm host fitness should depress densities of their hosts. However, parasites that alter host traits may increase host density via indirect ecological interactions. Here, we show how depression of foraging rate of infected hosts can produce such a hydra effect. Using a foraging assay, we quantified reduced foraging rates of a zooplankton host infected with a virulent fungal parasite. We then parameterized a dynamical model of hosts, parasites, and resources with this foraging function, showing how foraging depression can create a hydra effect. Mathematically, the hydra arose when increased resource productivity exceeded any increase in resource consumption per host. Therefore, the foraging-mediated hydra effect more likely emerged (1) for hosts that strongly control logistic-like resources and (2) during larger epidemics of moderately virulent parasites. We then analyzed epidemics from 13 fungal epidemics in nature. We found evidence for a foraging-mediated hydra effect: large outbreaks depressed foraging rate and correlated with increased densities of both algal resources and *Daphnia* hosts. Therefore, depression of the foraging rate of infected hosts can produce higher host densities even during epidemics of parasites that increase host mortality. Such hydras might prevent the collapse of host populations but also could produce higher densities of infected hosts.

Keywords: compensatory population growth, feeding behavior, host-parasite, hydra effect, illness-mediated anorexia, trait-mediated indirect effect.

Introduction

Disease epidemics can drive declines in host populations (Anagnostakis 1982; Lessios et al. 1984; Daszak et al. 1999), trigger conservation crises for wildlife such as mammals (Frick et al. 2015; Roelke-Parker et al. 1996; Lazenby et al. 2018) and birds (Hochachka and Dhondt 2000; Cooper et al. 2009; McClure et al. 2020), and even sometimes drive hosts extinct (amphibians; Vredenburg et al. 2010). Disease outbreaks can also damage economically valuable crops (Fry and Goodwin 1997), pollinators (Brosi et al. 2017), and livestock (Cleaveland et al. 2001). Even worse, climate change can further exacerbate disease epidemics (Altizer et al. 2013; Shocket et al. 2018; Sanderson and Alexander 2020). Therefore, it is imperative to identify when, where, and why parasites depress the density of their hosts during epidemics.

Typically, we predict that parasites depress host density because infection exacts virulent costs to host fitness. Indeed, infection often can increase the mortality rate and/or decrease the fecundity of infected hosts. Simple disease models illustrate how those two factors can lower host density relative to that under disease-free conditions (Anderson and May 1979, 1981). Furthermore, that harm can become amplified by higher transmission of disease (which can lead to higher prevalence of infection). Higher transmission results from higher per capita exposure and/or susceptibility (the product of which is called the "transmission rate"; Dwyer and Elkinton 1993; Strauss et al. 2018). Additionally, higher transmission can occur in more enriched systems that support higher density of hosts (assuming density-dependent spread of disease; Johnson et al. 2010). Therefore, we might expect larger depression of host density when virulent parasites reach higher prevalence.

On the other hand, these effects of disease outbreaks on host density might reverse if infection depresses the foraging rate of hosts. Many parasites lower the foraging rate of hosts (Hite and Cressler 2019; Strauss et al. 2019; Hite et al. 2020). At first glance, such foraging depression—whether a defense strategy or fitness cost of infection (Hite et al. 2020)—might seem to exacerbate declines in host density during epidemics. After all, lower intake of energy, when coupled with reduced survivorship and/or fecundity from infection, might harm fitness of hosts even more (all else equal). However, here we show that foraging depression can sometimes increase host density through a hydra effect (Abrams 2009). This outcome requires that hosts must strongly control a dynamic resource and that the resource must reach highest productivity at intermediate density (e.g., growing logistically or logistic-like; Schröder et al. 2014). When those conditions are met, foraging reduction can increase the density, and hence the production, of resources through indirect feedbacks (Schröder et al. 2014). Those increases in resource production can then compensate for increased energetic demands of hosts (a consequence of virulence). When the shift in resource production exceeds that in resource consumption, a foraging-mediated hydra effect emerges, leading to higher host density in the presence of parasites—even during very large outbreaks.

Here, we illustrate this foraging-mediated hydra mechanism using a freshwater system with a zooplankton host (*Daphnia dentifera*). This host can strongly depress an algal resource that reaches highest production at intermediate density. This host becomes infected by a fungus that predominantly lowers survival (Hall et al. 2010) rather than fecundity (unlike, e.g., the bacterium *Pasteuria*; Auld et al. 2012). In this study, we demonstrate that infection also lowers the foraging rate of hosts in an experiment, particularly as the final transmission stage of the fungus (spores) accumulate within the body cavity. We then parameterized a foraging depression function and incorporated it into a dynamical model. The model revealed how epidemics can drive higher host density (similar to how predators can increase prey density through changes in foraging behavior; Peacor and Werner 2001; Schröder et al. 2014). This foraging-mediated hydra effect becomes more likely as epidemics become larger (e.g., with higher density of spores within hosts and higher carrying capacity of the resource) and with stronger foraging depression. Conversely, it becomes less likely with higher virulence on survival. Finally, a survey of fungal epidemics in lakes showed that larger epidemics (with greater infection prevalence) yielded higher parasite production per host. We estimated the depression in foraging due to disease in those lakes and found that lower foraging correlated with joint increases of algal and zooplankton populations during epidemics. Taken together, this combination of experiments, dynamical modeling, and field surveys demonstrates how foraging depression can increase host density during epidemics of parasites that kill their hosts.

Study System and a Function for Foraging Depression (A Model Competition)

Disease System

The focal host, the zooplankton *Daphnia dentifera*, strongly grazes on phytoplankton in many lakes throughout the Midwest of the United States (Tessier and Woodruff 2002). Hosts ingest infectious propagules (spores) of the parasitic fungus *Metschnikowia bicuspidata* while foraging on small (<80-μm) phytoplankton (Hall et al. 2007b). As the parasite fills its host's hemolymph with spores (Green 1974; Ebert 2005), it reduces host growth, fecundity, and survivorship (Hall et al. 2009b). Death of the infected host releases spores into the water to then infect new hosts. Sometimes, epidemics of this fungus reduce host density and indirectly increase the density of the algal resource via a trophic cascade (Duffy 2007; Hall et al. 2011). At other times, host density remains high during epidemics (Duffy and Hall 2008; Hall et al. 2011).

Foraging Rate Experiment: Methods

We estimated foraging rate using an experiment, summarized only briefly here (for details, see sec. 1 of the appendix, available online). We measured feeding rate in individuals of cohorts of uninfected and infected hosts. To create a gradient in body size (host length, L_H) and spore yield (σ), we measured food consumption by individuals of progressively older age cohorts (which, in the infected class, corresponded with longer time since infection and greater spore loads). Thus, we placed individual hosts into small tubes containing their algal food, allowed them to graze for a short period of time (4 h), measured the remaining food using a fluorometer, and estimated length using a dissecting microscope. We verified infection status by smashing hosts to release spores contained in their body. These spores represent the final life stage of the parasite; their presence indicates terminal infection (Merrill et al. 2019).

Candidate Functions for Foraging Depression

We statistically competed foraging functions linking three mechanisms—infection status, body size (host length, L_H), and spore yield (σ)—to per capita "foraging" rate, $f(L_H, \sigma)$, for three host genotypes. The eight candidate foraging functions created from these mechanisms varied in complexity (table 1). Functions 1a–4a were fitted assuming a shared foraging coefficient (f or $\hat{f}$) for both infected and uninfected classes. For functions 1b–4b, we estimated parameters f_j or $\hat{f}_j$ separately for each infection class j (enabling

Table 1: Results of the model competition to estimate foraging rate, $f(L_H, \sigma)$

Function number (mechanism)	Foraging rate, $f(L_H, \sigma)$[a]	k[b]	ΔAIC[c]	Akaike weight (w)[d]
1a (null)	f	6	474.6	8.7×10^{-104}
1b (status only)	f_j	12	356.2	1.5×10^{-45}
2a (size only)	$\hat{f}L_H^2$	6	357.1	4.6×10^{-78}
2b (status and size)	$\hat{f}_j L_H^2$	12	138.3	9.1×10^{-31}
3a (spores only)	$f\left(1 - \alpha\left(\frac{\sigma}{L_H^3}\right)\right)$	9	349.0	1.6×10^{-76}
3b (status and spores)	$f_j\left(1 - \alpha\left(\frac{\sigma}{L_H^3}\right)\right)$	15	116.3	5.7×10^{-26}
4a (size and spores)	$\hat{f}L_H^2\left(1 - \alpha\left(\frac{\sigma}{L_H^3}\right)\right)$	9	144.7	7.1×10^{-47}
4b (status, size, spores)	$\hat{f}_j L_H^2\left(1 - \alpha\left(\frac{\sigma}{L_H^3}\right)\right)$	15	0	1.00

Note: Foraging functions 1a–4a fit a common "foraging" parameter (f or size-independent $\hat{f}$) to infected and uninfected hosts together for each genotype (i.e., no infection status mechanism). In functions 1b–4b, foraging parameters (f_j or $\hat{f}_j$) were estimated separately for uninfected (f_S or $\hat{f}_S$) and infected (f_I or $\hat{f}_I$) hosts in each genotype (enabling the infection status mechanism). Size-independent parameters $\hat{f}$ and $\hat{f}_j$ allow for differences in feeding due to size (the size mechanism). Body length, L_H, and spore yield, σ, were measured empirically (fig. 1d–1f). We estimated the linear sensitivity coefficient (α; mm^3 spore^{-1}) for each genotype (the spores mechanism).

[a] Per capita rates; technically, this is the "clearance rate" in theory for foraging ecology. Units for f_j: L day^{-1}; units for size-independent $\hat{f}_j$: L mm^{-2} day^{-1}.

[b] Number of parameters estimated for all three genotypes, including a variance parameter estimated for each infection class (functions 1b–4b) and genotype (all functions). For uninfected hosts, $\alpha = 0$ (i.e., not estimated) in functions 3a–4b.

[c] The best foraging function (4b) has an Akaike information criterion (AIC) of -212.5; hence, for 4b, ΔAIC $= 0$. Functions with ΔAIC > 10 have essentially no support.

[d] The probability that the foraging function is the best among those under consideration.

the status mechanism). In function 1 (null), per capita foraging rate (f) is a single parameter (f). Hence, 1a is a true null, and 1b (status only) layers in the infection status mechanism. In function 2a (size only), a size-independent foraging coefficient ($\hat{f}$) is multiplied by L_H^2. Hence, feeding area is proportional to the surface area of hosts, a common assumption in grazing models (Hall et al. 2007b; Kooijman 2010). This foraging function allows size differences between infection classes to influence foraging (the size mechanism). Function 2b (status and size) includes the infection status and size mechanisms. In function 3a (spores only), foraging rate drops as spores fill the body volume of infected hosts, $\propto L_H^3$ (i.e., as σ/L_H^3 increases, governed by coefficients α and γ; the spores mechanism). Foraging function 3b combines the status and spores mechanisms, while function 4a (size and spores) combines the effects of size with the spore-mediated foraging depression. Finally, the most complex variant, function 4b (status, size, spores) combines all three mechanisms. We inserted the best-fitting foraging function (hereafter, "best"), assuming constant host length, into the dynamic epidemiological model (see "Dynamical Model: Foraging Depression Can Produce a Hydra during Epidemics" be-

low; figs. 3, A3; figs. A1–A4 are available online). Additionally, this best function enabled us to estimate the depression of foraging during epidemics (see "Field Survey: Evidence for the Hydra during Large Epidemics in Nature" below; figs. 6, A4).

Parameterization and Competition of the Foraging Function

We used maximum likelihood and information theoretic methods to parameterize and compete the foraging functions, implemented with Matlab (ver. 7.8 R2009a; MathWorks). We estimated parameters by fitting a model of algal loss through time due to foraging (Sarnelle and Wilson 2008; Strauss et al. 2019):

$$\ln(A_t) = \ln(A_0) - \frac{f(L_H, \sigma)t_E}{V + \varepsilon}, \quad (1)$$

where A_t is the concentration of algae remaining at the end of the grazing period of length t; A_0 is the concentration of algae in ungrazed reference tubes at time t_E; $f(L_H, \sigma)$ is one

of the foraging functions (potentially) incorporating host length, L_H, and spore yield, σ (table 1); V is the volume in the tube; and errors (ε) were normally distributed. (While it is technically "clearance rate" in foraging theory, the "foraging" label here avoids confusion with the immunological meaning of clearance.) We estimated parameters using maximum likelihood and competed functions using standard information criteria (the Akaike information criterion [AIC], ΔAIC, and Akaike weights, w, for each model; see table 1; Burnham and Anderson 2002). We estimated the 95% confidence interval around the parameters of the best-fitting foraging function (4b, status, size, spores) with 10,000 bootstraps (table A1, available online). We also compared parameters between host genotypes using 9,999 permutations (Gotelli and Ellison 2004; table A1). The slope and intercept of a regression of observed versus predicted ($\ln(A_0/A_t)V/t$) remaining algae were close to 1 and 0, respectively, indicating good performance (observed $= 1.007 \times$ predicted $- 0.056 + \varepsilon$; $R^2 = 0.55$; Piñeiro et al. 2008).

Outcome of the Competition among Foraging Functions: Results

Parasite infection reduced the foraging rate of hosts, particularly during the later stages of infection (fig. 1a–1c). In those later stages, fungal spores filled the body cavity of its host (fig. 1d–1f). Furthermore, infection stunted the body size of sick hosts relative to that of uninfected hosts of the same age and genotype (fig. 1d–1f). As a result, the best function for parasite-induced foraging depression (function 4b, status, size, spores; tables 1, A1; figs. 1, A1) was as follows:

for uninfected hosts:
$$f_S(L_H) = \hat{f}_S\,L_H^2, \tag{2a}$$

for infected hosts:
$$f_I(L_H, \sigma) = \hat{f}_I\,L_H^2\left(1 - \alpha\left(\frac{\sigma}{L_H^3}\right)\right), \tag{2b}$$

where $\hat{f}_S$ and $\hat{f}_I$ are size-independent per capita foraging rates (the status mechanism), L_H is host body length (the
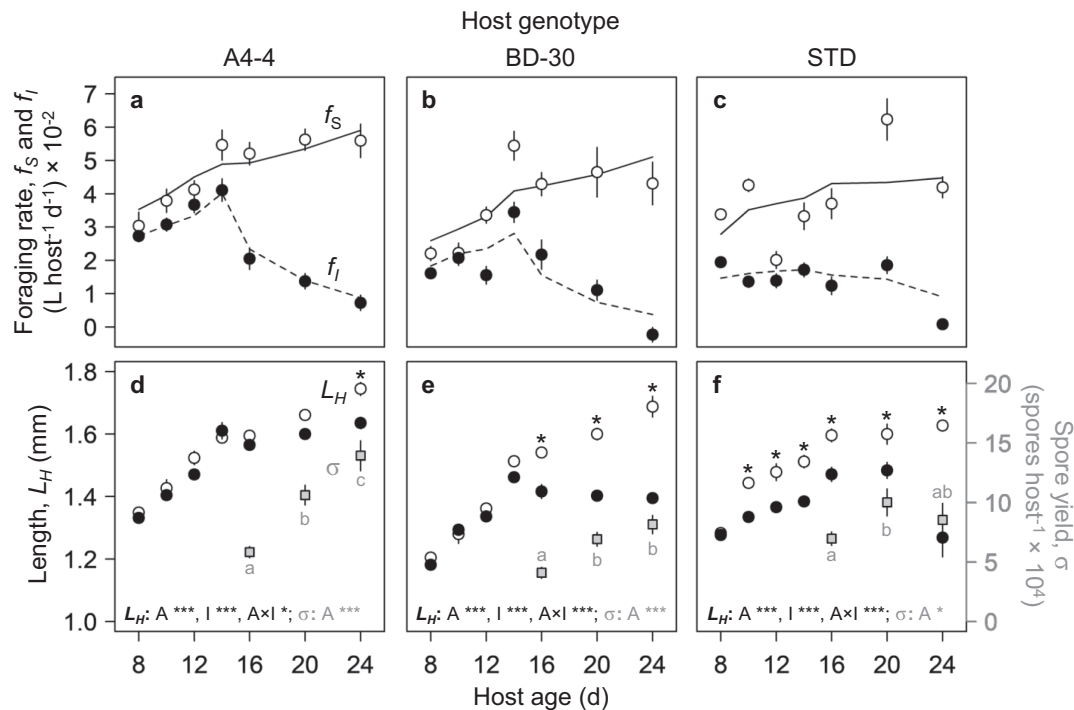

Figure 1: Parasites depress host foraging rate, *f*, as functions of host length, L_H, and spore yield, σ. *a–c*, Foraging rate (mean $\pm$ 1 SE) of uninfected (f_S, white circles) and infected (f_I, black circles) individuals of three genotypes of a zooplankton host with the best-fitting foraging function (f_S, eq. [2a], solid lines; f_I, eq. [2b], dashed lines; model 4b of table 1). *a*, *b*, For genotypes A4-4 and BD-30, the foraging rate increased with age (and, thus, body size) of uninfected hosts and those at early stages of infection. Foraging then dropped as infected hosts filled with spores. *c*, Infection reduced foraging rate earlier for the STD genotype. Foraging data were calculated from observed resource densities (see sec. 1 of the appendix). *d–f*, Host length (L_H) of uninfected (white circles) and infected (black circles) hosts and spore yield (σ, gray squares) of three host genotypes: A4-4 (*d*), BD-30 (*e*), and STD (*f*). Spore yield also increased with age (noting a few [$N = 3$] smaller STD hosts at 24 days). *P* values are from generalized linear model–based tests of age (*A*), infection (*I*), and their interaction ($A \times I$) on length and of age on spore yield (*$^*P < .05$, $^{***}P < .001$). Asterisks above body length points indicate significant post hoc pairwise differences (Tukey's) between infection classes. Letters denote significant post hoc differences in spore yield between age classes. Points: means $\pm$ 1 SE. See table A1 for parameter estimates.

size mechanism), σ is the spore load per infected host, and α is a linear sensitivity coefficient that governs depression of feeding as spores fill the host's body cavity (the spores mechanism). These equations (eqq. [2a], [2b]) capture how body size increased foraging. For uninfected hosts, foraging scaled with surface area ($\propto L_H^2$; eq. [2a]; fig. 1, solid lines, white circles). For infected hosts (eq. [2b]; fig. 1, dashed lines, black circles), foraging rate also increased with surface area, although at a slower rate (since $\hat{f}_I < \hat{f}_S$; table A1), but it decreased as their body volume ($\propto L_H^3$) filled with spores (σ; fig. 1).

Dynamical Model: Foraging Depression Can Produce a Hydra during Epidemics

Structure of the Dynamical Model

We inserted the best foraging function (eqq. [2]) into a dynamical model. This model could then delineate conditions leading to foraging-mediated hydras versus trophic cascades during epidemics (eq. [3]; table 2; fig. 2):

susceptible:
$$\frac{dS}{dt} = e(f_S S + f_I I)A - dS - uf_S SZ, \quad (3a)$$

infected:
$$\frac{dI}{dt} = uf_S SZ - (d + v)I, \quad (3b)$$

propagules:
$$\frac{dZ}{dt} = \sigma(A)(d + v)I - mZ$$
$$- (f_S S + f_I I)Z, \quad (3c)$$

where $\sigma(A) = \dfrac{\sigma_1 A}{h + A}, \quad (3d)$

resources:
$$\frac{dA}{dt} = r_m A\left(1 - \frac{A}{K}\right) - (f_S S + f_I I)A. \quad (3e)$$

Table 2: Variables, parameters, and functions used in the dynamical model of host-parasite-resource interactions (eqq. [3]), with default values or ranges (when applicable)

Symbol	Meaning	Default values/range	Unit
A	Density of resource of host	...	mg C L^{-1}
I	Density of infected hosts	...	host L^{-1}
N	Density of hosts: $N = S_i + I$	...	host L^{-1}
S	Density of susceptible hosts	...	host L^{-1}
t	Time	...	day
Z	Density of parasite propagules (spores)	...	spore L^{-1}
d	Background death rate of hosts	.03	day^{-1}[a]
e	Conversion efficiency of host	8.5	mg C^{-1}[b]
L_H	Body length of host	1.4	mm
$\hat{f}_S$	Size-independent foraging rate for susceptible hosts	.0178	L mm^{-2} day^{-1}
$\hat{f}_I$	Size-independent foraging rate for infected hosts	.0131	L mm^{-2} day^{-1}
α	Sensitivity coefficient of foraging of infected hosts	2.86×10^{-5} (fig. 3*j*: .35 to 2.8×10^{-5})	mm^3 spore^{-1}
f_a	Mean foraging rate of hosts: $f_a = (1 - p) f_S + p f_I$	...	L day^{-1}
f_S	Foraging rate of susceptible hosts (eq. [2a])	.035	L day^{-1}
f_I	Foraging rate of infected hosts (eq. [2b])	0 (bounded) to .035	L day^{-1}
h	Half-saturation constant, spore yield	.015	mg C L^{-1}[c]
K	Carrying capacity of resources	.1 to 3.0	mg C L^{-1}
m	Mortality of spores, Z	.8	day^{-1}[d]
p	Prevalence of infection: $I/(S_i + I)$	...	unitless
PP	Primary production: PP $= r_m A(1 - A/K)$	...	mg C L^{-1} day^{-1}
r_m	Maximum per capita growth rate of A	.8	day^{-1}[a]
u	Susceptibility	.0004	host spore^{-1}[e]
v	Virulence on survival	.07 (fig. 3*i*: .03 to .15)	day^{-1}
$\sigma(A)$	Spore yield (eq. [3d])	...	spore host^{-1}
σ_1	Maximum spore yield	1.0 to 2.5×10^3 (fig. 3*i*, 3*j*: 1.5×10^4)	spore host^{-1} mg C^{-1}

[a] Reasonable value for this host and algae.
[b] Yields a reasonable instantaneous birth rate, b_S, of 0.30 day^{-1} for uninfected hosts at 1.0 mg C L^{-1} (where $b_S = ef_S A$; Hall et al. 2010).
[c] Reasonable value for this host (Strauss et al. 2015).
[d] A high loss rate due to solar radiation (Overholt et al. 2012) and other sources (e.g., consumption by nonfocal hosts; Hall et al. 2009a).
[e] Yields an infection risk (transmission rate, β) of 1.4×10^{-5} L spore^{-1} day^{-1} (where $\beta = uf_S$).

Genesis of the foraging-mediated hydra during disease epidemics.
Disease epidemics can increase host density, N^*, via foraging-mediated hydras.

Equilibrial host density, N^*, is a **ratio**

host density $N^* = \dfrac{PP^*}{f_a A_i^*}$ — primary production

— food consumption

Hydras occur if epidemics increase PP^* more than $f_a A_i^*$

Three requirements enable the foraging-mediated hydra during epidemics.

(1) Epidemics increase **resource density, A_i^***:

Resources during epidemics

virulence   prevalence

$A_i^* = \dfrac{d+vp^*}{e[(1-p^*)f_S+p^*f_I]}$

conversion   foraging rate of S foraging rate of I

Mean foraging rate:
$f_a = (1-p^*)\,f_S + p^*\,f_I$

Foraging depression:
if $f_S > f_I$ then $f_a \downarrow$ as $p^* \uparrow$

Infection is **virulent** when: $v > 0$

A_i^* increases with foraging depression and virulence

Resource density without parasites (at boundary b) is $A_b^* = d/(e\,f_S)$.
Resource density during epidemics (at interior i), A_i^*, exceeds A_b^*, increasing with: higher disease prevalence, p^*; higher virulence of infection, v; and / or when infection causes stronger foraging depression, $f_S > f_I$.

(2) More resources elevate **resource production, PP^***:

Because the resource grows logistically, its production is hump-shaped:
$PP^* = r_m A^* (1 - A^* / K)$. PP is maximized when $K/2$. Therefore:

Hosts weakly depress A: If $A_b^* > K/2$, hydras are not possible.

Here, when $A_i > A_b^*$, $PP\downarrow$ during epidemic.

No hydra: $A_b^* > K/2$
Weakly depress

Hydra possible: $A_b^* < K/2$
Strongly depress

Hosts strongly depress A: If $A_b^* < K/2$, hydras become possible.

When $A_i > A_b^*$, $PP\uparrow$ in cases 1 and 2;

however, $PP\downarrow$ in case 3 (so no hydra)

Primary production, PP

Resource density, A

(3) **Consumption**, $f_a A_i^*$, cannot increase too much.

Food consumption per host, $f_a A_i^*$, is the product of mean foraging rate, f_a, and resource density, A_i^*. As infection prevalence, p^*, increases:

(A) resources increase most for virulent parasites ($v>0$) that depress foraging ($f_S > f_I$) …

Resources, A_i^*

Consumption, $f_a A^*$

Prevalence of infection, p

(B) … but foraging consumption, $f_a A_i^*$, increases only for virulent parasites (esp. higher v);

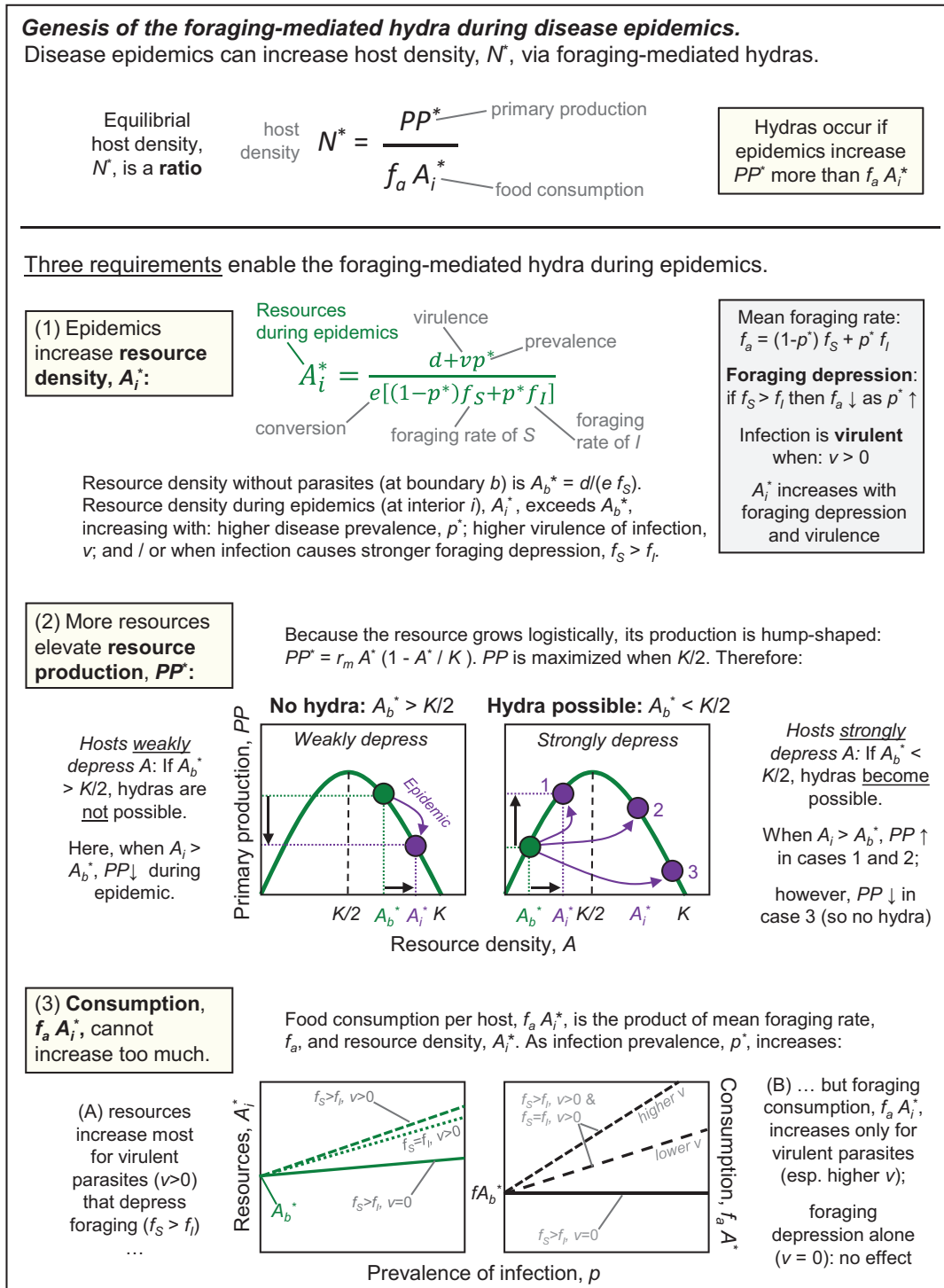foraging depression alone ($v = 0$): no effect

Figure 2: Explanation of the conditions that enable a foraging-mediated hydra effect during disease epidemics.

Susceptible hosts (S; eq. [3a]) feed nonselectively at rate f_S on algal resources (A); infected hosts (I) feed at reduced rate f_I. Feeding rates followed the best-fitting foraging function described above (4b, status, size, spores; eqq. [2]). For sim-

plicity, we assumed that hosts feed with a linear functional response. Ingested food is converted into offspring with efficiency e. Susceptible hosts (S) then die at background rate d or become infected following exposure (at rate f_S) to

spores (Z), with per-spore susceptibility u. Infected hosts (I; eq. [3b]) die from infection (at enhanced rate $d + v$); they cannot recover. Total host density (N) sums both host classes ($S + I$). Spores (Z; eq. [3c]) are released from dead hosts; spore yield, $\sigma(A)$, increases with algal resources (A) but saturates (with maximum σ_1 and half-saturation constant h; eq. [3d]). Spores are lost at background rate m and via consumption by both host classes. Algal resources (eq. [3e]) grow logistically (at maximum per capita rate r_m and carrying capacity K) and are consumed by both host classes.

We simulated the model over a range of algal carrying capacity, K, and sensitivity of spore production to resources, σ_1. We parameterized it using biologically reasonable values for this system (table 2) and estimates of $\hat{f}_S$, $\hat{f}_I$, and α for the BD-30 genotype (eqq. [2]; fig. 1; table A1; assuming adult size $L_H = 1.4$ mm for both uninfected and infected hosts). Qualitatively similar results emerged using parameters from other genotypes. This dynamical model is not analytically tractable; thus, we simulated it (using a standard adaptive step integrator in Matlab) for 1,000 days. We then averaged densities of the state variables over time points from $t = 1{,}000$–$2{,}000$ days. In the focal, biologically relevant region of parameter space shown here, the state variables reached a stable steady state by this time period (confirmed by solving for equilibria numerically with a rootfinder). We calculated threshold combinations of K and mortality virulence (v) and of K and the sensitivity coefficient (α) that yielded foraging-mediated hydras (higher A and N [$N\uparrow$]) versus cascades (higher A but lower N [$N\downarrow$]) during epidemics. In each case, the threshold was found numerically (using a rootfinder) when host density at the boundary equilibrium (eqq. [A2]) equaled host density at the endemic (interior) equilibrium (solved for numerically). Assuming that susceptible hosts enjoyed a higher size-independent foraging rate than infected hosts ($\hat{f}_S > \hat{f}_I$; the status mechanism), we found threshold levels of virulence mortality (v) at which hydra effects arose, either with sensitivity of foraging to spore accrual ($\alpha > 0$; the spores mechanism) or not ($\alpha = 0$; no spores mechanism). Then, at a given level of v, we found threshold levels of sensitivity to spore accrual (α) at which hydra effects arose, due to either both mechanisms of foraging depression ($\hat{f}_S > \hat{f}_I$, $\alpha > 0$; the status and spores mechanisms together) or only the effect of spores on foraging ($\hat{f}_S = \hat{f}_I$, $\alpha > 0$; the spores mechanism alone). (None of these combinations included the size mechanism, since we did not model body size dynamically.)

Prediction of Hydra from the Dynamical Model: Results

Parasite-induced foraging depression can trigger a trait-mediated hydra effect (fig. 3). Our dynamical model (eqq. [3]; table 2) predicts that increasing the carrying capacity of algal resources (K; x-axis) or the maximum spore yield per infected host (σ_1; contours) should increase the equilibrial prevalence of infection (p^*; fig. 3a). During larger epidemics, the average per capita death rate of hosts ($d + p^* v$) increases as a result of virulent effects of the parasite on host survivorship (fig. 3b). Larger epidemics also yield greater density of resources, A, at equilibrium (A_i^*; fig. 3c). Since this density is also the minimal resource requirement of hosts, it increases with heightened mortality of hosts and foraging depression (figs. A2, A3). More resources fuel greater within-host spore yield, $\sigma(A_i^*)$ (eq. [3d]; fig. 3d). Higher spore yield enhances the spread of disease and boosts epidemic size, but it also depresses the mean foraging rate of hosts, f_a (where $f_a = (1 - p^*)f_S + p^* f_I$; f_S and f_I follow eqq. [2a] and [2b], respectively; fig. 3e).

The model predicts either trophic cascades or foraging-mediated hydras during epidemics—the outcome for host density depends on the relative effect of disease on resource production versus that on per capita resource consumption of hosts. The increase in resource density (due to virulent depression of foraging and survival) increases primary production, $PP^* = r_m A^* (1 - A^*/K)$—as long as carrying capacity of the resource, K, is high enough ($A_b^* > K/2$; see fig. 2; secs. 2, 3 of the appendix; fig. 3f). Food consumption per host, $f_a A_i^*$, also increases with K and maximum spore yield σ_1 (fig. 3g). Host density, N^*, then increases or decreases (relative to disease-free conditions; thick gray) depending on the tension between the responses of PP^* and $f_a A_i^*$ (fig. 3h; see also fig. 2; secs. 2, 3 of the appendix; fig. A3). At lower K, virulence on survival dominates, decreasing host density. At higher K, foraging depression and higher primary production increase host density. Therefore, the model predicts that larger epidemics may increase host density when parasites reduce the feeding rate of their hosts enough in sufficiently enriched systems (for more details, see fig. 2; secs. 2, 3 of the appendix). Furthermore, the foraging-mediated hydra effect should arise more readily when parasites are less lethal to their hosts (lower v; figs. 3i, 4a, 4b), especially when infected hosts have lower baseline foraging rates (the status mechanism; $\hat{f}_S > \hat{f}_I$) and their foraging is additionally depressed by within-host spore growth (the spores mechanism; $\alpha > 0$; fig. 4a; note that the status mechanism [$\hat{f}_S > \hat{f}_I$] enables the hydra effect even without the spores mechanism [$\alpha = 0$]; fig. 4b). Also, at a given virulence level (v), the hydra effect is more likely (i.e., can occur at lower K) when spore accrual more strongly suppresses foraging rate (higher α; figs. 3j, 4c–4f). The hydra effect occurs at lower α with the status mechanism ($\hat{f}_S > \hat{f}_I$; fig. 4c, 4d) than without it ($\hat{f}_S = \hat{f}_I$; i.e., the spores mechanism alone; fig. 4e, 4f)—therefore, both the status mechanism and the spores mechanism of foraging depression ($\alpha > 0$, $\hat{f}_S > \hat{f}_I$) enhance the hydra effect. Finally, the depression of host foraging rate
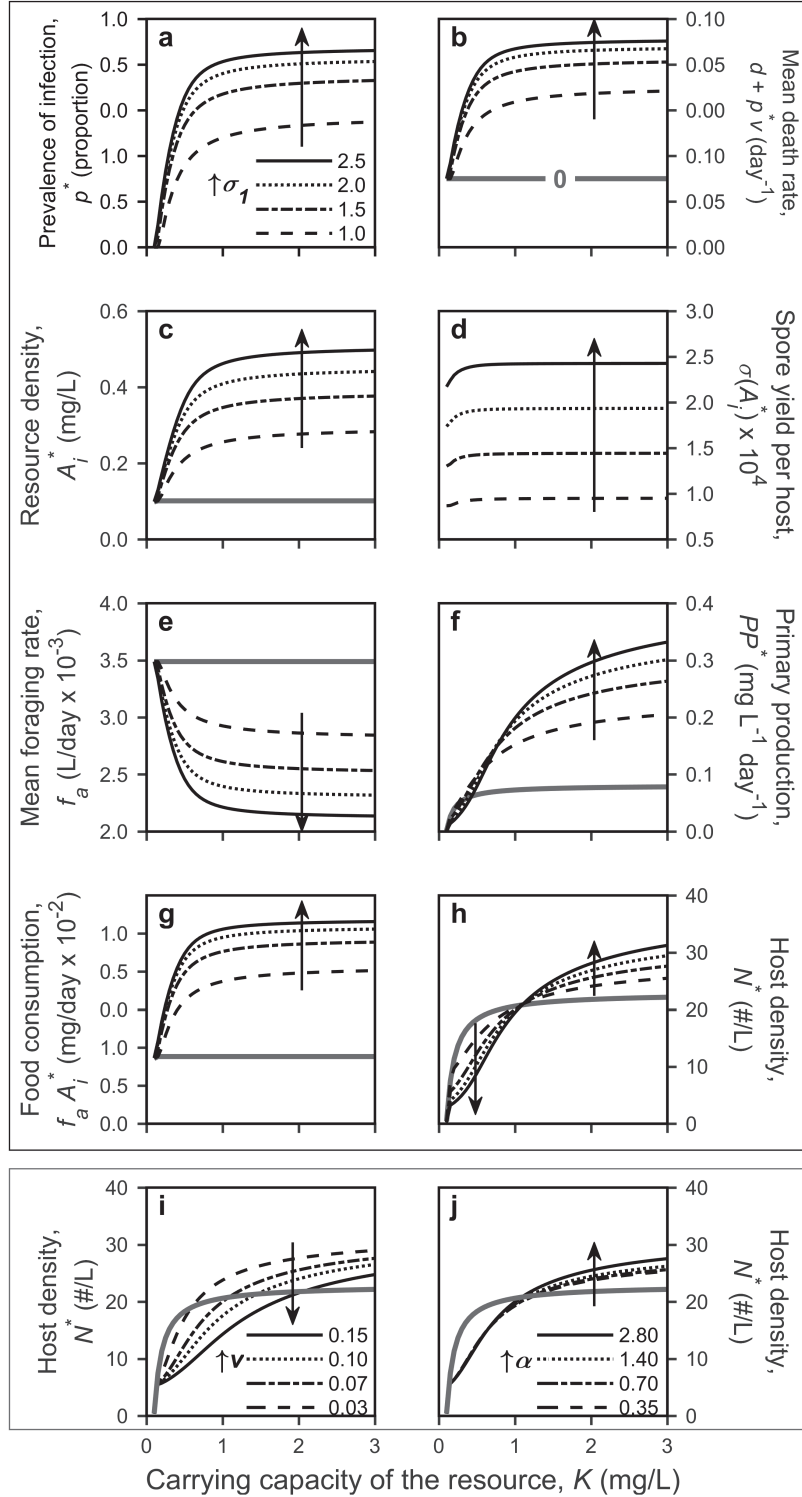
Figure 3: Fully dynamical model reveals a trait-mediated hydra effect through depression of foraging rate. Equilibrial density of hosts, N^*, can increase during epidemics of a virulent parasite over gradients of carrying capacity, K (x-axis). Disease-free states are denoted by thick gray contours. For epidemics, arrows across contours show increasing values of maximal spore yield σ_1 (spore host^{-1} mg C^{-1} × 10^4; a–h); virulence, v (day^{-1}; i); or sensitivity coefficient of foraging of infected hosts, α (mm^3 spore^{-1}; j; i and j are boxed and shaded for contrast). a, Equilibrial disease prevalence (proportion infected, p^*); b, mean per capita death rate ($d + vp^*$); c, algal resources (A_i^*); d, spore yield

may also drive higher infection prevalence, through mechanisms involving higher spore production (due to increased resources) and lower spore losses (due to depressed removal from the environment by infected hosts; see sec. 3 of the appendix and fig. A3a–A3c).

Field Survey: Evidence for the Hydra during Large Epidemics in Nature

Estimation of Infection Prevalence, Algal Density, Spore Yield: Methods

We sampled 13 lakes in southern Indiana (Greene and Sullivan Counties) weekly from August until the first week of December 2010. Here, we present data from the epidemic season (end of September through mid-November). On each sampling visit, we pooled three bottom-to-surface tows of a Wisconsin net (13 cm in diameter, 153-μm mesh). From this sample, we estimated prevalence infection (p) by diagnosing at least 400 live *Daphnia dentifera* at ×20–50 magnification (Ebert 2005). From this sample, we estimated the prevalence of infection in the adult size class only (p_a). We also measured the body length (L_H) of uninfected and infected adult hosts (typically >20 of each class). Additionally, we estimated the average spore yield (σ) of infected hosts (typically 5–40 hosts, pooled together). We estimated host density using preserved (60%–75% ethanol) samples, pooling three additional bottom-to-surface net tows. Finally, we indexed the density of "edible' (<80-μm Nitex screening) algae in the epilimnion using narrowband filters on a Trilogy fluorometer (Turner Designs) following chilled ethanol extraction (Webb et al. 1992; Welschmeyer 1994).

Index of Foraging Depression and Death Rate: Methods

For each lake population, we calculated an index of disease-induced foraging depression of adult hosts using (1) prevalence and spore yield data (fig. A4a), (2) body size of uninfected and infected adults (fig. A4b), and (3) parameters from the best foraging function (eqq. [2]; table A1; $\hat{f}_S$, $\hat{f}_I$, α; genotypes labeled 1–3 in fig. A4b–A4d). We only summarize this calculation here (for details, see sec. 4 of the appendix). For the infected class, we assumed that each infected adult shared the mean spore yield estimate for that lake-date combination (σ). With these parameters and

data, we calculated the mean foraging rate of adults, f_a, as the mean foraging rate of each infection class of adults ($\overline{f_{a,S}}, \overline{f_{a,I}}$) weighted by the prevalence of infection of adults, p_a; hence, $f_a = (1 - p_a)\overline{f_{a,S}} + p_a\overline{f_{a,I}}$ (see eqq. [A11a]–[A11c], incorporating the status, size, and spores mechanisms). Next, we calculated the mean foraging rate of adults assuming differences in mean body size only, f_0 (i.e., the size mechanism alone; eq. [A11d]). The index of foraging depression, FD, was then: FD $= (f_0 - f_a)/f_0 \times 100\%$ (eq. [A11e]; fig. A4d). For each lake, we averaged this index, calculated at each sampling date, for each set of genotype-derived parameters (1–3); then we averaged those three separate genotype-specific estimates to produce one value of FD per lake (see fig. A4 for sample calculations). We also estimated the average death rate of hosts during epidemics using the egg ratio method (for details, see sec. 4 of the appendix).

Joint Algal-Host Response Index: Methods

We calculated a joint algal-host response index to test qualitative predictions of the dynamical model. If epidemics trigger a hydra, we expect both hosts and resources to increase, particularly during larger epidemics. To quantify a simple index, we first estimated the linear slopes of hosts and algal resources through time (e.g., fig. 5a, 5b). We then standardized these slopes for both hosts and resources by dividing each slope by the standard deviation of the slopes among lakes. After this standardization, the slope estimates then became unitless, and slopes for both hosts and resources fell along a similar scale. We then multiplied these two standardized slopes to produce a joint response index for each lake (fig. 5c, 5d). When both algae and hosts increased through time, this product was positive (e.g., the large epidemic in Goodman Lake; fig. 5a, 5c), consistent with a hydra effect. However, if only one of these (algae or hosts) increased through time, the product was negative (e.g., the small epidemic in Long Lake; fig. 5b, 5d). Densities of algae and hosts never both decreased through time (i.e., positive values arose only from two positive slopes, not two negative ones).

Signature of the Trait-Mediated Hydra Effect in the Field: Results

In the field survey, we detected the hydra pattern anticipated by the dynamical model. Infected hosts yielded more

---

($\sigma(A_i^*)$); *e*, mean foraging rate ($f_a = [1 - p^*]f_S + p^*f_I$); *f*, primary production (PP$^* = r_m A^*(1 - A^*/K)$; *g*, resource consumption per host ($f_a A_i^*$); *h*, total host density (N^*). Hydras arise at higher K (N^* higher with disease than without [thick, gray]) and become larger with higher σ_1. The hydra effect was accentuated by lower virulence on survivorship (v [day^{-1}]; *i*) and higher feeding sensitivity (α [×10^{-5} mm^3 spore^{-1}]; *j*). Therefore, hydras were more likely with higher carrying capacity of the resource (K) and for parasites that depress mortality less strongly (lower v) and foraging more strongly (higher α). See figure 2 for additional explanation, table 2 for default parameters, and sections 2 and 3 of the appendix for more analysis.
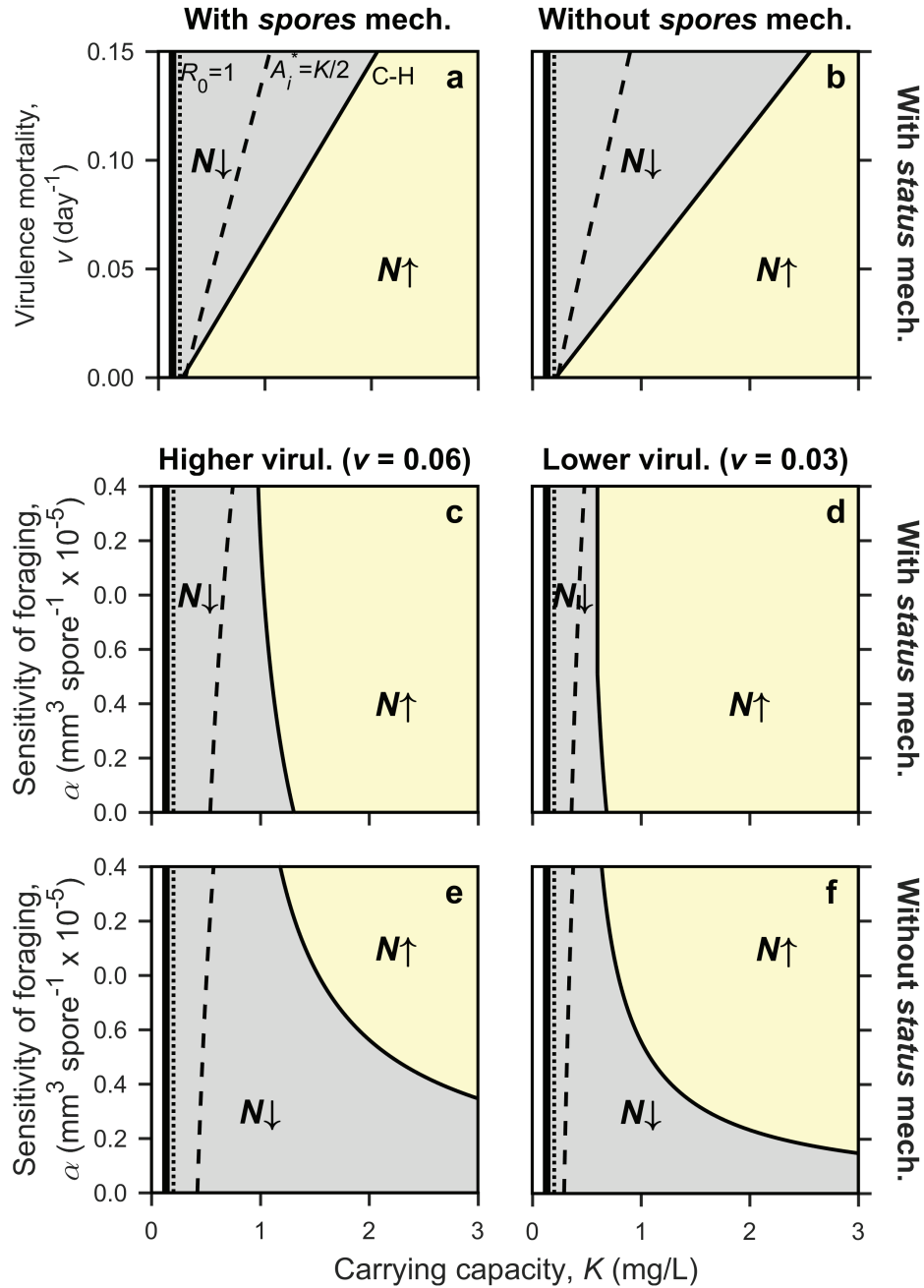
Figure 4: Parameter space predicting trophic cascades (host density decreases; gray, $N\downarrow$) or foraging-mediated hydra (yellow, $N\uparrow$) over gradients of carrying capacity (K) of the resource (see also fig. 2). Curves: "C-H," solid line, border between cascade and hydra; $A_i^* = K/2$ for disease (dashed) and disease-free (dotted) equilibrium; $R_0 = 1$ at thick solid. *a*, *b*, Foraging-mediated hydras occur at a given K if virulence mortality, v, is not too high (below solid line). Scenarios assuming susceptible hosts feed faster than infecteds (the status mechanism; $\hat{f}_S > \hat{f}_I$): foraging is sensitive to spores (the spores mechanism 2; $\alpha > 0$; *a*) and is not (without the spores mechanism; $\alpha = 0$; *b*). *c*–*f*, Foraging-mediated hydras are predicted, at a given K, when the coefficient of sensitivity of foraging (α) exceeds a threshold. This threshold incorporates the status mechanism ($\hat{f}_S > \hat{f}_I$) at higher (*c*) or lower (*d*) virulence or does not incorporate it ($\hat{f}_S = \hat{f}_I$) at higher (*e*) or lower (*f*) virulence. All parameters follow the defaults in table 1.
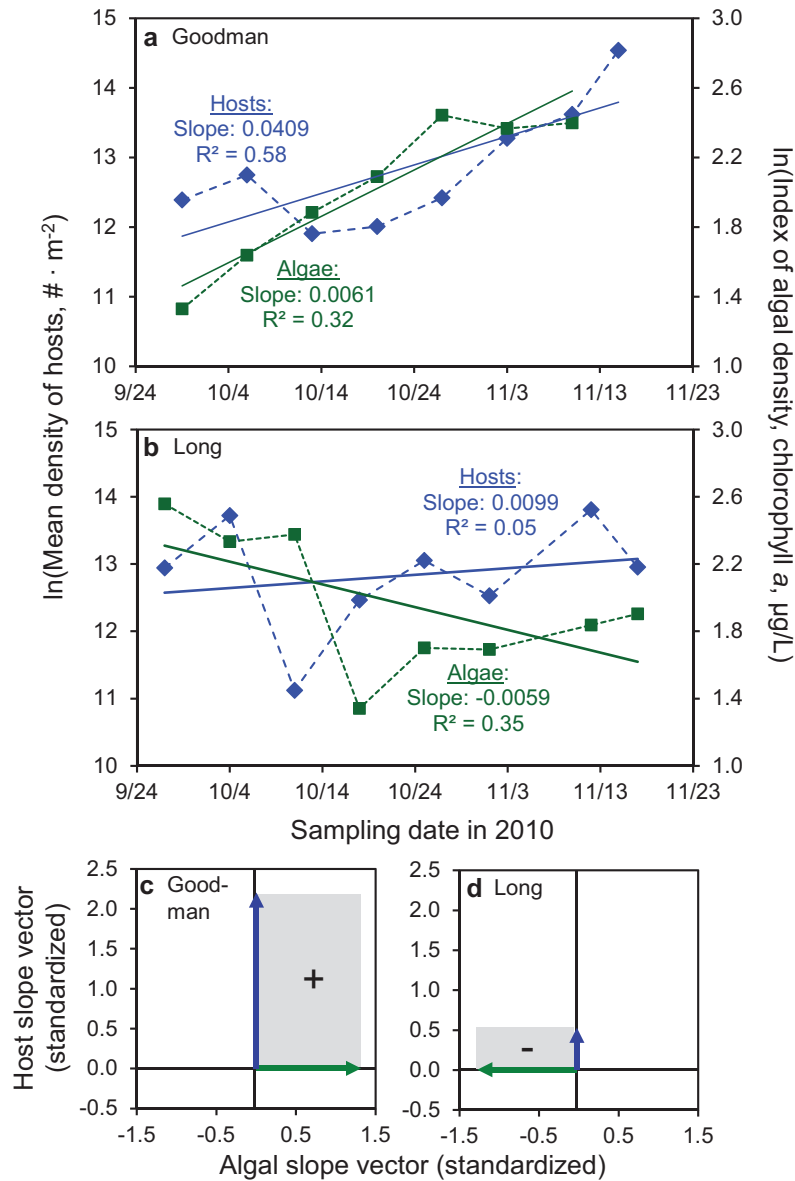
Figure 5: Changes in hosts and algal resources create a joint algal-host response. *a*, During the large epidemic in Goodman Lake (maximum infection prevalence: 48.6%; see also fig. A4), both hosts and algal resources increased through time. *b*, During Long Lake's small epidemic (maximum prevalence: 5.2%), hosts increased but algal resources declined. *c*, *d*, The joint algal-host response index for Goodman (*c*) and Long (*d*) is calculated as the product of these slopes, first standardized (see text); the magnitude is denoted by the gray area. This joint index is presented in figure 6*c* and 6*d*.

spores in lakes with larger outbreaks (fig. 6*a*) and more algal resources (shown previously; Civitello et al. 2015). For lakes with greater spore loads, in turn, we estimated stronger depression of foraging by adult hosts (figs. 6*b*, A4). Lakes with stronger foraging depression then had greater values of the joint algal-host response index (figs. 5, 6*c*). Positive values of this index indicate a hydra (see above). As predicted then, the signal of the foraging-mediated hydra effect arose during larger epidemics (higher prevalence) with stronger for-

aging depression (fig. 6*c*, 6*d*). In contrast, the mean death rate (estimate of $d + p^* v$) was not correlated with the index of foraging depression ($R = 0.23$, $P = .42$) or the joint algal-host index ($R = 0.26$, $P = .35$).

Discussion

Undeniably, large epidemics of virulent parasites can depress host densities. However, here we show that indirect
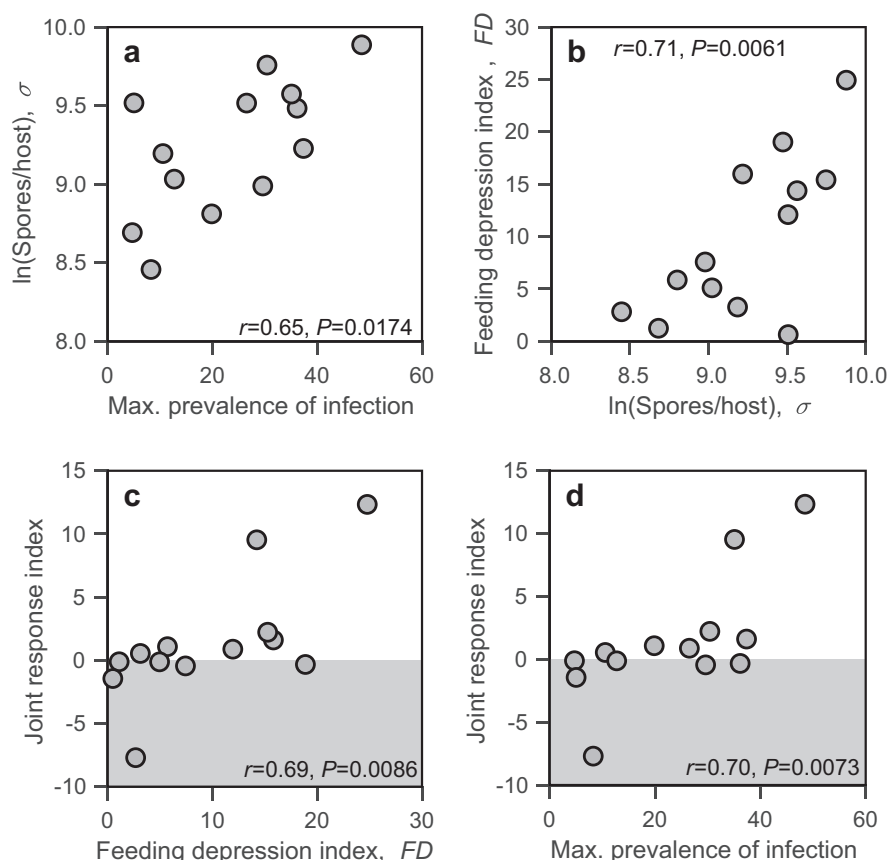
Figure 6: Evidence for a joint increase in densities of zooplankton (*Daphnia*) hosts and algal resources during natural fungal epidemics (a hydra). *a*, Infected hosts produced more spores (σ) during larger epidemics (higher maximum prevalence of infection, p_{max}). *b*, These greater spore loads depressed average per capita feeding rate of adult hosts, f_a (calculated using length, spores, and prevalence data; see fig. A4, eqq. [A11]). *c*, Stronger parasite-induced depression of foraging rate correlated with a larger index of joint algal-host response (fig. 5*c*, 5*d*) through time during epidemics. *d*, The joint algal-host response index was larger during bigger fungal outbreaks. Points are lake means. Pearson correlation coefficients (*r*) are accompanied by corresponding *P* values.

feedbacks between hosts and resources can drive the opposite pattern: host density can increase during outbreaks. More specifically, parasites that virulently depress the foraging rate of infected hosts can indirectly produce more hosts under certain conditions. Using a zooplankton-fungus-algal system, we show how infection by a virulent parasite depresses foraging of infected hosts. Then, using a dynamical model of host-parasite-resource interactions, we show when the foraging-mediated hydra effect should and should not arise (fig. 2). The model predicted hydras during larger epidemics that strongly depress foraging of hosts while, at the same time, not depressing fitness too much. We then turned to naturally occurring epidemics, finding support consistent with a foraging-mediated hydra effect. During larger epidemics, more spores accumulated in host bodies, which depressed foraging. Reduced foraging, in turn, correlated with a joint increase in hosts and algal resources—a signature of the hydra effect.

How and why does foraging depression produce the hydra? In the model, it works via two determinants of host density: the ratio of resource production and resource consumption per host (fig. 2; adapted from Schröder et al. 2014). Both components start with an increase in the minimal resource requirement of hosts (an indirect effect). Hosts require enough resources to offset increased mortality (resulting from virulence of infection) with reproduction (extending logic from Grover 1997). Reduced foraging further increased this requirement. The subsequent increase in resource density can elevate resource production (Case 2000). However, higher food density compensates for slower feeding, yielding no net change in per capita resource consumption. Therefore, foraging depression alone enhances the likelihood of hydra effects during epidemics. In this system, foraging depression arose via multiple mechanisms. Infected hosts had a lower feeding rate for a given size (the status mechanism), spore yield in host bodies

substantially diminished foraging (the spores mechanism), and infected hosts reached smaller size (the size mechanism, reducing feeding further). Higher density of resources released by the epidemic should exacerbate the spores mechanism (Hall et al. 2009b; Civitello et al. 2015). Finally, these hosts slow feeding when contacting parasite propagules (Hite et al. 2017; Strauss et al. 2019). Hence, in this plankton system, multiple mechanisms produce foraging depression. Since parasite-mediated foraging depression arises commonly in other systems as well (Hite and Cressler 2019; Hite et al. 2020), this foraging mechanism for a hydra may apply quite broadly.

Even with foraging depression, hydra effects may still not arise unless additional conditions are met (fig. 2). First, hosts must strongly control their resource. While *Daphnia* depresses its algal resources, not all hosts can similarly (Borer et al. 2005; Shurin and Seabloom 2005). Second, the subsequent increase in resource density must enhance resource productivity. Some resources follow a more donor-controlled, chemostat-style supply (Polis et al. 1997); in these cases, productivity drops as resource density increases, eliminating the hydra (see the appendix; Schröder et al. 2014). Notably, many experiments impose donor control on resources, eliminating the potential for foraging-mediated hydras as described here. Furthermore, sufficient enrichment is needed for higher density to increase resource productivity. Third, parasites cannot depress survivorship or fecundity (Hall et al. 2007a; Lafferty and Kuris 2009) too strongly. Those forms of virulence increase per host resource consumption, potentially overwhelming any increase in resource productivity. Fourth, epidemics must become large enough to trigger the requisite indirect effects to densities and traits. Our results suggest that these requirements are met in this planktonic system. It remains to be determined how many other systems can also produce a foraging-mediated hydra.

Where does this foraging-mediated hydra result fit within other behaviors of host-parasite-resource systems? First, hydras can arise via other mechanisms (Abrams and Matsuda 2005; Abrams 2009; Cortez and Abrams 2016). Increased mortality of hosts during epidemics could stabilize oscillatory host-resource cycles to increase host density. Here, the linear functional response of our model yielded stable dynamics (given the biological relevant parameters), obviating evaluation of this mechanism mathematically. Yet in the field, we also found no relationship between mean per capita death rate and the joint algal-host index (but for an example of increased mortality driving higher density in mosquitoes, see McIntire and Juliano 2018). Second, parasites can alternatively drive trophic cascades (Buck and Ripple 2017). In our model, cascades were more likely at lower productivity, for less sensitive foragers, and for more virulent parasites. Third, parasites can trigger "bio-

mass overcompensation" in their host. This outcome, assuming certain trait asymmetries between life stages of hosts, can increase the biomass of the life stage most readily infected (Schröder et al. 2009; de Roos and Persson 2013; Preston and Sauer 2020). Hopefully, a coherent theory will emerge that synthesizes these possibilities for hydras, cascades, and biomass overcompensation during epidemics.

Moving one step further, the foraging-mediated hydra effect should be integrated into a broader theory for the community ecology of disease. First, foraging depression by parasites should stabilize host-resource oscillations, providing another mechanism to produce a hydra effect (e.g., Hilker et al. 2009; Hurtado et al. 2014). Second, other food web interactors might stifle this foraging-mediated hydra. For instance, competitors of hosts could fix resources at their own minimal resource requirement (analogous to systems with inedible producers; Grover 1995). Therefore, resource competition might prevent hydras. Third, key trade-offs can influence the evolution of hosts during epidemics (Boots et al. 2009; Duffy and Forde 2009). This *Daphnia* host shows foraging-mediated relationships between fecundity and transmission rate (Hall et al. 2010; Auld et al. 2013) and between feeding rate and sensitivity to contact with spores (Strauss et al. 2019). Such relationships could interact with foraging-mediated hydras as hosts evolve during epidemics. Therefore, integration of the foraging-mediated hydra effect into the community and evolutionary ecology of disease seems likely to yield interesting insights.

The foraging-mediated hydra effect described here means that large outbreaks may indirectly cause increases in host density. Parasite-mediated foraging depression occurs in a diverse array of systems (Hite and Cressler 2019; Hite et al. 2020). Yet the foraging-mediated hydra here rests on a number of requirements, including that hosts strongly control resources, that resource productivity increases, and that infection only moderately increases mortality. It remains unknown how many other systems meet these conditions. However, it is important to note that these foraging-mediated hydra effects may produce desirable or undesirable outcomes. Hydras might prevent worrisome collapses in host density during large outbreaks. Yet they also increase the density of infected hosts, potentially elevating disease risk to humans (via contact with infected hosts) or spillover to other hosts. Future efforts should evaluate the frequency and magnitude of foraging-mediated hydra effects and their influence on disease and communities.

Statement of Authorship

R.M.P. conceived of the study and designed the experiment, with assistance from M.A.D. and S.R.H. R.M.P., M.S.S., J.H.O., B.C.P.L., H.S., and M.A.D. performed the experiment. S.R.H. and M.A.D. designed the field survey. S.R.H., R.M.P., and M.S.S. carried out the field survey. R.M.P. and S.R.H. did the modeling and analysis. R.M.P., S.R.H., and M.A.D. wrote the manuscript, and all authors contributed to later drafts.

Data and Code Availability

All data and code (R and Matlab) have been deposited in the Dryad Data Repository (https://doi.org/10.5061/dryad.np5hqbzsd; Penczykowski et al. 2021).

Literature Cited

Abrams, P. A. 2009. When does greater mortality increase population size? the long history and diverse mechanisms underlying the hydra effect. Ecology Letters 12:462–474.

Abrams, P. A., and H. Matsuda. 2005. The effect of adaptive change in the prey on the dynamics of an exploited predator population. Canadian Journal of Fisheries and Aquatic Sciences 62:758–766.

Altizer, S., R. S. Ostfeld, P. T. J. Johnson, S. Kutz, and C. D. Harvell. 2013. Climate change and infectious diseases: from evidence to a predictive framework. Science 341:514–519.

Anagnostakis, S. L. 1982. Biological control of chestnut blight. Science 215:466–471.

Anderson, R. M., and R. M. May. 1979. Population biology of infectious diseases: part I. Nature 280:361–367.

———. 1981. The population dynamics of microparasites and their invertebrate hosts. Philosophical Transactions of the Royal Society B 291:451–524.

Auld, S. K. J. R., S. R. Hall, and M. A. Duffy. 2012. Epidemiology of a *Daphnia*-multiparasite system and its implications for the Red Queen. PLoS ONE 7:e39564.

Auld, S. K. J. R., R. M. Penczykowski, J. H. Ochs, D. C. Grippi, S. R. Hall, and M. A. Duffy. 2013. Variation in costs of parasite resistance among natural host populations. Journal of Evolutionary Biology 26:2479–2486.

Boots, M., A. Best, M. R. Miller, and A. White. 2009. The role of ecological feedbacks in the evolution of host defence: what does theory tell us? Philosophical Transactions of the Royal Society B 364:27–36.

Borer, E. T., E. W. Seabloom, J. B. Shurin, K. E. Anderson, C. A. Blanchette, B. Broitman, S. D. Cooper, et al. 2005. What determines the strength of a trophic cascade? Ecology 86:528–537.

Brosi, B. J., K. S. Delaplane, M. Boots, and J. C. de Roode. 2017. Ecological and evolutionary approaches to managing honeybee disease. Nature Ecology and Evolution 1:1250–1262.

Buck, J. C., and W. J. Ripple. 2017. Infectious agents trigger trophic cascades. Trends in Ecology and Evolution 32:681–694.

Burnham, K. P., and D. R. Anderson. 2002. Model selection and multimodel inference: a practical information-theoretic approach. 2nd ed. Springer, New York.

Case, T. J. 2000. An illustrated guide to theoretical ecology. Oxford University Press, New York.

Civitello, D. J., R. M. Penczykowski, A. N. Smith, M. S. Shocket, M. A. Duffy, and S. R. Hall. 2015. Resources, key traits and the size of fungal epidemics in *Daphnia* populations. Journal of Animal Ecology 84:1010–1017.

Cleaveland, S., M. K. Laurenson, and L. H. Taylor. 2001. Diseases of humans and their domestic mammals: pathogen characteristics, host range and the risk of emergence. Philosophical Transactions of the Royal Society B 356:991–999.

Cooper, J., R. J. M. Crawford, M. S. De Villiers, B. M. Dyer, G. J. G. Hofmeyr, and A. Jonker. 2009. Disease outbreaks among penguins at sub-Antarctic Marion Island: a conservation concern. Marine Ornithology 37:193–196.

Cortez, M. H., and P. A. Abrams. 2016. Hydra effects in stable communities and their implications for system dynamics. Ecology 97:1135–1145.

Daszak, P., L. Berger, A. A. Cunningham, A. D. Hyatt, D. E. Green, and R. Speare. 1999. Emerging infectious diseases and amphibian population declines. Emerging Infectious Diseases 5:735–748.

de Roos, A. M., and L. Persson. 2013. Population and community ecology of ontogenetic development. Princeton University Press, Princeton, NJ.

Duffy, M. A. 2007. Selective predation, parasitism, and trophic cascades in a bluegill-*Daphnia*-parasite system. Oecologia 153:453–460.

Duffy, M. A., and S. E. Forde. 2009. Ecological feedbacks and the evolution of resistance. Journal of Animal Ecology 78:1106–1112.

Duffy, M. A., and S. R. Hall. 2008. Selective predation and rapid evolution can jointly dampen effects of virulent parasites on *Daphnia* populations. American Naturalist 171:499–510.

Dwyer, G., and J. S. Elkinton. 1993. Using simple models to predict virus epizootics in gypsy moth populations. Journal of Animal Ecology 62:1–11.

Ebert, D. 2005. Ecology, epidemiology and evolution of parasitism in *Daphnia*. US National Library of Medicine, National Center for Biotechnology Information, Bethesda, MD.

Frick, W. F., S. J. Puechmaille, J. R. Hoyt, B. A. Nickel, K. E. Langwig, J. T. Foster, K. E. Barlow, et al. 2015. Disease alters macroecological patterns of North American bats. Global Ecology and Biogeography 24:741–749.

Fry, W. E., and S. B. Goodwin. 1997. Re-emergence of potato and tomato late blight in the United States. Plant Disease 81:1349–1357.

Gotelli, N. J., and A. M. Ellison. 2004. A primer of ecological statistics. Sinauer, Sunderland, MA.

Green, J. 1974. Parasites and epibionts of *Cladocera*. Transactions of the Zoological Society of London 32:417–515.

Grover, J. P. 1995. Competition, herbivory, and enrichment: nutrient-based models for edible and inedible plants. American Naturalist 145:746–774.

———. 1997. Resource competition: population and community biology series. Springer, Boston, MA.

Hall, S. R., C. Becker, and C. E. Cáceres. 2007*a*. Parasitic castration: a perspective from a model of dynamic energy budgets. Integrative and Comparative Biology 47:295–309.

Hall, S. R., C. R. Becker, M. A. Duffy, and C. E. Cáceres. 2010. Variation in resource acquisition and use among host clones creates key epidemiological trade-offs. American Naturalist 176:557–565.

———. 2011. Epidemic size determines population-level effects of fungal parasites on *Daphnia* hosts. Oecologia 166:833–842.

Hall, S. R., C. R. Becker, J. L. Simonis, M. A. Duffy, A. J. Tessier, and C. E. Cáceres. 2009*a*. Friendly competition: evidence for a dilution effect among competitors in a planktonic host-parasite system. Ecology 90:791–801.

Hall, S. R., J. L. Simonis, R. M. Nisbet, A. J. Tessier, and C. E. Cáceres. 2009*b*. Resource ecology of virulence in a planktonic host-parasite system: an explanation using dynamic energy budgets. American Naturalist 174:149–162.

Hall, S. R., L. Sivars-Becker, C. Becker, M. A. Duffy, A. J. Tessier, and C. E. Cáceres. 2007*b*. Eating yourself sick: transmission of disease as a function of foraging ecology. Ecology Letters 10:207–218.

Hilker, F. M., M. Langlais, and H. Malchow. 2009. The Allee effect and infectious diseases: extinction, multistability, and the (dis-) appearance of oscillations. American Naturalist 173:72–88.

Hite, J. L., and C. E. Cressler. 2019. Parasite-mediated anorexia and nutrition modulate virulence evolution. Integrative and Comparative Biology 59:1264–1274.

Hite, J. L., R. M. Penczykowski, M. S. Shocket, K. A. Griebel, A. T. Strauss, M. A. Duffy, C. E. Cáceres, et al. 2017. Allocation, not male resistance, increases male frequency during epidemics: a case study in facultatively sexual hosts. Ecology 98:2773–2783.

Hite, J. L., A. C. Pfenning, and C. E. Cressler. 2020. Starving the enemy? feeding behavior shapes host-parasite interactions. Trends in Ecology and Evolution 35:68–80.

Hochachka, W. M., and A. A. Dhondt. 2000. Density-dependent decline of host abundance resulting from a new infectious disease. Proceedings of the National Academy of Sciences of the USA 97:5303–5306.

Hurtado, P. J., S. R. Hall, and S. P. Ellner. 2014. Infectious disease in consumer populations: dynamic consequences of resource-mediated transmission and infectiousness. Theoretical Ecology 7:163–179.

Johnson, P. T. J., A. R. Townsend, C. C. Cleveland, P. M. Glibert, R. W. Howarth, V. J. McKenzie, E. Rejmankova, et al. 2010. Linking environmental nutrient enrichment and disease emergence in humans and wildlife. Ecological Applications 20:16–29.

Kooijman, S. A. L. M. 2010. Dynamic energy budget theory for metabolic organisation. Cambridge University Press, Cambridge.

Lafferty, K. D., and A. M. Kuris. 2009. Parasitic castration: the evolution and ecology of body snatchers. Trends in Parasitology 25:564–572.

Lazenby, B. T., M. W. Tobler, W. E. Brown, C. E. Hawkins, G. J. Hocking, F. Hume, S. Huxtable, et al. 2018. Density trends and demographic signals uncover the long-term impact of transmissible cancer in Tasmanian devils. Journal of Applied Ecology 55:1368–1379.

Lessios, H. A., D. R. Robertson, and J. D. Cubit. 1984. Spread of *Diadema* mass mortality through the Caribbean. Science 226:335–337.

McClure, K. M., R. C. Fleischer, and A. M. Kilpatrick. 2020. The role of native and introduced birds in transmission of avian malaria in Hawaii. Ecology 101:e03038.

McIntire, K. M., and S. A. Juliano. 2018. How can mortality increase population size? a test of two mechanistic hypotheses. Ecology 99:1660–1670.

Merrill, T. E. S., S. R. Hall, L. Merrill, and C. E. Cáceres. 2019. Variation in immune defense shapes disease outcomes in laboratory and wild *Daphnia*. Integrative and Comparative Biology 59:1203–1219.

Overholt, E. P., S. R. Hall, C. E. Williamson, C. K. Meikle, M. A. Duffy, and C. E. Cáceres. 2012. Solar radiation decreases parasitism in *Daphnia*. Ecology Letters 15:47–54.

Peacor, S. D., and E. E. Werner. 2001. The contribution of trait-mediated indirect effects to the net effects of a predator. Proceedings of the National Academy of Sciences of the USA 98:3904–3908.

Penczykowski, R. M., M. S. Shocket, J. Housley Ochs, B. C. P. Lemanski, H. Sundar, M. A. Duffy, and S. R. Hall. 2021. Data from: Virulent disease epidemics can increase host density by depressing foraging of hosts. American Naturalist, Dryad Digital Repository, https://doi.org/10.5061/dryad.np5hqbzsd.

Piñeiro, G., S. Perelman, J. P. Guerschman, and J. M. Paruelo. 2008. How to evaluate models: observed vs. predicted or predicted vs. observed? Ecological Modelling 216:316–322.

Polis, G. A., W. B. Anderson, and R. D. Holt. 1997. Toward an integration of landscape and food web ecology: the dynamics of spatially subsidized food webs. Annual Review of Ecology and Systematics 28:289–316.

Preston, D. L., and E. L. Sauer. 2020. Infection pathology and competition mediate host biomass overcompensation from disease. Ecology 101:e03000.

Roelke-Parker, M. E., L. Munson, C. Packer, R. Kock, S. Cleaveland, M. Carpenter, S. J. Obrien, et al. 1996. A canine distemper virus epidemic in Serengeti lions (*Panthera leo*). Nature 379:441–445.

Sanderson, C. E., and K. A. Alexander. 2020. Unchartered waters: climate change likely to intensify infectious disease outbreaks causing mass mortality events in marine mammals. Global Change Biology 26:4284–4301.

Sarnelle, O., and A. E. Wilson. 2008. Type III functional response in *Daphnia*. Ecology 89:1723–1732.

Schröder, A., L. Persson, and A. M. de Roos. 2009. Culling experiments demonstrate size-class specific biomass increases with mortality. Proceedings of the National Academy of Sciences of the USA 106:2671–2676.

Schröder, A., A. van Leeuwen, and T. C. Cameron. 2014. When less is more: positive population-level effects of mortality. Trends in Ecology and Evolution 29:614–624.

Shocket, M. S., A. T. Strauss, J. L. Hite, M. Sljivar, D. J. Civitello, M. A. Duffy, C. E. Cáceres, et al. 2018. Temperature drives epidemics in a zooplankton-fungus disease system: a trait-driven approach points to transmission via host foraging. American Naturalist 191:435–451.

Shurin, J. B., and E. W. Seabloom. 2005. The strength of trophic cascades across ecosystems: predictions from allometry and energetics. Journal of Animal Ecology 74:1029–1038.

Strauss, A. T., A. M. Bowling, M. A. Duffy, C. E. Cáceres, and S. R. Hall. 2018. Linking host traits, interactions with competitors and disease: mechanistic foundations for disease dilution. Functional Ecology 32:1271–1279.

Strauss, A. T., D. J. Civitello, C. E. Cáceres, and S. R. Hall. 2015. Success, failure and ambiguity of the dilution effect among competitors. Ecology Letters 18:916–926.

Strauss, A. T., J. L. Hite, D. J. Civitello, M. S. Shocket, C. E. Cáceres, and S. R. Hall. 2019. Genotypic variation in parasite avoidance behaviour and other mechanistic, nonlinear components of transmission. Proceedings of the Royal Society B 286:20192164.

Tessier, A. J., and P. Woodruff. 2002. Cryptic trophic cascade along a gradient of lake size. Ecology 83:1263–1270.

Vredenburg, V. T., R. A. Knapp, T. S. Tunstall, and C. J. Briggs. 2010. Dynamics of an emerging disease drive large-scale amphibian population extinctions. Proceedings of the National Academy of Sciences of the USA 107:9689–9694.

Webb, D. J., B. K. Burnison, A. M. Trimbee, and E. E. Prepas. 1992. Comparison of chlorophyll *a* extractions with ethanol and dimethyl sulfoxide/acetone, and a concern about spectrophotometric phaeopigment correction. Canadian Journal of Fisheries and Aquatic Sciences 49:2331–2336.

Welschmeyer, N. A. 1994. Fluorometric analysis of chlorophyll *a* in the presence of chlorophyll *b* and pheopigments. Limnology and Oceanography 39:1985–1992.

both among-host competition and evolution of transmission potential of parasites. American Naturalist 184:S77–S90.

Bottrell, H. H., A. Duncan, Z. M. Gliwicz, E. Grygierek, A. Herzig, A. Hillbricht Ilkowska, H. Kurasawa, et al. 1976. A review of some problems in zooplankton production studies. Norwegian Journal of Zoology 24:419–456.

Chen, C. T., and F. J. Millero. 1977. Use and misuse of pure water PVT properties for lake waters. Nature 266:707–708.

Duffy, M. A., S. R. Hall, A. J. Tessier, and M. Huebner. 2005. Selective predators and their parasitized prey: are epidemics in zooplankton under top-down control? Limnology and Oceanography 50:412–420.

Hall, S. R., M. A. Duffy, A. J. Tessier, and C. E. Cáceres. 2005. Spatial heterogeneity of daphniid parasitism within lakes. Oecologia 143:635–644.

Klüttgen, B., U. Dulmer, M. Engels, and H. T. Ratte. 1994. ADaM, an artificial freshwater for the culture of zooplankton. Water Research 28:743–746.

Merrill, T. E. S., and C. E. Cáceres. 2018. Within-host complexity of a plankton-parasite interaction. Ecology 99:2864–2867.

References Cited Only in the Online Enhancements

Auld, S. K. J. R., S. R. Hall, J. H. Ochs, M. Sebastian, and M. A. Duffy. 2014. Predators and patterns of within-host growth can mediate
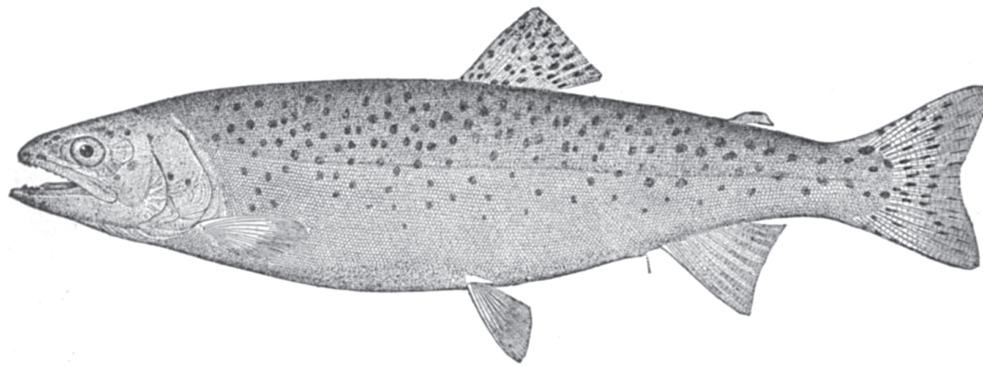
"North America and Asia have at least one species of Salmo in common—a small-scaled species,—*S. purpuratus*. This is the most widely-distributed and the most variable of our species." From "Distribution and Some Characters of the Salmonidæ" by Tarleton H. Bean (*The American Naturalist*, 1888, 22:306–314).